Electromechanical Energy Conversion Systems (EECS)
Niroo Research Institute (NRI)
Vol. 3, No. 1, Autumn 2024, 29-35
DOI: 10.30503/eecs.2024.462133.1053
Original Article

The Effect of Cation Distribution on Magnetic Properties of Zn_{1-x} $Fe_{1.2}$ $[(Mn_xNi_{1-x})_{0.8}$ $(Co_xCu_{1-x})_{0.2}]_{x+0.8}O_4$ Ferrites and Determination of Optimal Magnetization

Sareh Shafiee[1,2*]

Abstract

Zn_{1-x} $Fe_{1.2}$ $[(Mn_xNi_{1-x})_{0.8}$ $(Co_xCu_{1-x})_{0.2}]_{x+0.8}O_4$ (where x=0, 0.4 and 0.8) ferrites were synthesis via the co-precipitation process. The scope of this research is the inquiry of magnetized behavior of ferrites based on cation dispensation between sites (A and B) and a discussion of the substitution result of Mn, Cu, Ni, and Co ions on the particle size and magnetized parameters of Zn ferrites.

Using X-ray diffraction (XRD) the single-phase cubic formation of ferrites was certified. The mean sizes of crystallite ferrites were obtained 6-9 nm. Also, the lattice constant were calculated 8.386-8.399 Å. These parameters were increased with growing x composition. The field emission scanning electron microscopy revealed that the mean particle size for all samples were 11-14 nm. From M-H curves, the magnetization was determined in a magneto field of 8 kOe. The magnetization of un-calcined ferrites was not saturated. To reach saturation magnetization (M_s), all ferrites were calcined at 900°C. The study indicated the increment in M_s with the enhancement of x contents. This behavior was discussed via the core-shell model, theory belong to Neel, and the raplacement of sites by cations. The research evidented the maximum and minimum magnetization on the calcined ferrite x = 0.8 and the un-calcined sample with x = 0.0, respectively. The quality of particles was measured via the squareness ratio. Also, the changes of coercivity (H_c) were discussed. With growing x values, the H_c for calcined samples were reduced. It was described by the multi-domain formation of spinel ferrites. The x=0 calcined ferrite evidenced maximum H_c. Therefore, amongst samples, x=0.8 ferrite, due to maximum M_s and minimum H_c, may be useful for applications with high-frequency.

Keywords: NiCuMnCoZn ferrites, Calcination, Magnetic behaviors, Core-shell, Neel's theory, Coercivity.

Received Date:2024-06-10 ; Revised Date:2024-09-07 ; Accepted Date: 2024-09-11.

Introduction

Spinel ferrites, use in various applications with high-frequency such as transformer cores, , ferrofluids, the absorbed microwave, electrical devices and geberators, and antennas for radio receivers. Because their magnetic, thermal electrical, dielectric, or catalytic behaviors are unique. These features contain wide magnetization, resistance, and Curie temperature, more magnetocrystalline anisotropy, useful chemical stability. [1-3].

The magnetized behaviors of ferrites are related to the interchange and replacement of cations amongst both A and B sites, synthesis method, chemical composition, and particle size [4, 5]. Replacement A and B by cations causes the categorization of spinel ferrites into normal, inverse, and mixed. The spinel structure of $ZnFe_2O_4$ is normal. Because the A and B sites in this ferrite contain Zn^{2+} and Fe^{3+} ions, respectively. Although, this type of spinel formation indicates poor magnetic features, the replacement of metal ions on zinc ferrites cause to the redistribution of ions in the A and B sites. Besides, with mechanical treatment and heating Zn^{2+} and Fe^{3+} ions may become disordered over the A and B sites and change the magneto features [6]. Various techniques are used for the synthesis the ferrites, which are selected by the targeted applications and desired behaviors of these ferrites [7]. Amongst methods like ball milling, citrate, hydrothermal, sol-gel process, solid-state method, and co-precipitation process [8], a co-precipitation technique usually is usefull, because of the simple method at low temperature and controllability of crystallite size [9]. Some studies have indicated the dependency of cations distribution on the particle size [9, 10]. The magnetized order of the spins on surface has role in ferrite magnetized behaviors because of the formation of magnetic dead layer and the increment

[1]*Electronic and Instrumentation Research Department, Niroo Research Institute (NRI), Tehran, Iran*
[2]*Department of Applied Science, Malek Ashtar University of Technology, Shahin Shahr, Iran*
**Corresponding author, Email:sshafiee@nri.ac.ir*

in surface-to-volume ratio with reduction size of particles [11].

The unsaturated nature of magnetization can be ascribed to the size of particles, and the diffusion of cations in the crystal. To reach saturated magnetization, the samples are calcined at 900 ◦C. The M_s for all ferrites calculated at 900 °C is more. The changes of M_s are related to the sizes of particle and the diffusion of cations.

Many researchers have focused on improving the magnetic features of Zn ferrites by substituting different metal ions [12-17]. Shahane et al. [15] have reported the influence of nickel's concentration on the structure and magnetic features of $Ni_xZn_{1-x}Fe_2O_4$. The research showed the ferromagnetic behavior of the $x = 0.5$ ferrite and the superparamagnetic behavior for $x = 0.1$ and $x = 0.3$. Also, the sizes of crystals enhanced from 12 to 17 nm corresponding $x = 0.1$ to $x = 0.5$. The nickel cation have key role in determination the zinc ferrite magneto feature [15]. Dimri Rao et al. [17] have reported the influence of compositional variation on the magneto behavior of NiCuZn ferrite with the formula of $Ni_{0.6-x}Cu_xZn_{0.4}Fe_2O_4$. Replacement of Ni by Cu in the B site resulted a reduction in M_s. The values of calculated saturation magnetization showed an enhancement with increasing Cu cations [17]. In work, the influence of Mn, Cu, Ni, and Co substituted on the magneto behaviors of Zinc ferrite with the formula of $Zn_{1-x}Fe_{1.2}[(Mn_xNi_{1-x})_{0.8}(Co_xCu_{1-x})_{0.2}]_{x+0.8}O_4$ (where x= 0, 0.4 and 0.8) is investigated. These ferrites were synthesized by the co-precipitation technic and were calcined at 900 ◦C to reach saturation magnetization. The scope of research is (a) investigation of the magnetic features of samples related to distribution of cations on A and B sites; (b) a discussion of the substitution effect of Mn, Cu, Ni, and Co ions on the particle size and magnetic parameters of Zn ferrites; (c) Compare the magnetic parameters obtained for samples with different research under previous conditions.

1. EXPERIMENTAL

For preparation $Zn_{1-x}Fe_{1.2}[(Mn_xNi_{1-x})_{0.8}(Co_xCu_{1-x})_{0.2}]_{x+0.8}O_4$ by co-precipitation method, x changes from 0.0 to 0.8, the stoichiometric amounts of raw materials, like $NiCl_2.6H_2O$ (Merck, 98%), $ZnCl_2.4H_2O$ (Merck, 98%), $CuCl_2.2H_2O$ (Merck, 99%), $MnCl_2.4H_2O$ (Merck, 98%), $CoCl_2.6H_2O$ (Merck, 99%) and $FeCl_3.6H_2O$ (Merck, 99%), were used. The preparation process of spinel ferrites has been reported in various works [15-18]. The raw materials dissolved in deionized water were mixed. Then they were stirred at 80◦C for 1 h. the stoichiometric amount of NaOH dissolved in deionized water was stirred at 80◦C. The measured PH of the material was 10. To obtain chemical homogeneity, the mixture was stirred at 80◦C for 2 h. Then, the precipitated particles were washed with pure water. After reaching the pH = 7, the solution was dried at 100◦C for 12 h in an air atmosphere overnight.

To study the magnetic features of samples, they were calcined at 900◦C for 2 h. Finally, the magnetic properties of un-calcined and calcined samples were analyzed and compared. The phase structure, lattice constant, and crystallite sizes were analyzed by XRD diffractometer. The mean crystallite size was obtained using Scherer's formula. The particle size was calculated by field emission scanning electron microscopy (FESEM).The magnetic measurements were reported in a field of 8 kOe using an alternating gradient force magnetometer (AGFM). The magnetic features and coercivity were calculated.

2. RESULTS AND DISCUSSION

3.1. Structural properties

XRD spectrum for un-calcined ferrites are shown in Fig. 1. The diffractograms of samples prepared with the co-precipitation route reveal the reflections of (111), (220), (311), (400), (331), (511), (440), and (620). A comparison peak position with the mentioned standard (JCPDS card No: 01-022-1086) confirms the single-phase cubic structure of ferrites [19]. Using XRD data and the Scherrer-Debye formula the average crystallite sizes and lattice constant were evaluated, as listed in Table 1.

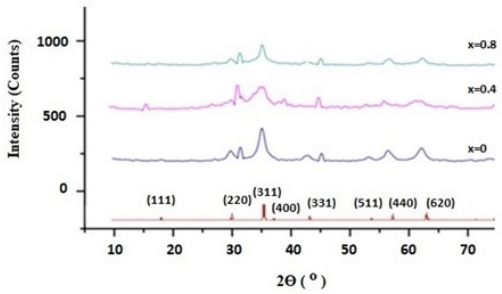

Fig. 1. XRD patterns of un-calcined samples of $Zn_{1-x}Fe_{1.2}[(Mn_xNi_{1-x})_{0.8}(Co_xCu_{1-x})_{0.2}]_{x+0.8}O_4$ (x= 0, 0.4 and 0.8)

TABLE. 1. Contents of D, a, d on un-calcined samples

Composition (x)	0.0	0.4	0.8
mean Crystallite Size(D), nm	6	7	9
Lattice Constant (a), Å	8.388	8.390	8.399
mean Particle Size (d), nm	11	12	14

The changes of mean crystallite size and lattice constant depend on x concentration are shown in Fig. 2. It is observed that the mean crystallite size is increased 6-9 nm as the enhancement of x values. Also, the lattice constant was calculated about 8.386-8.399 Å.

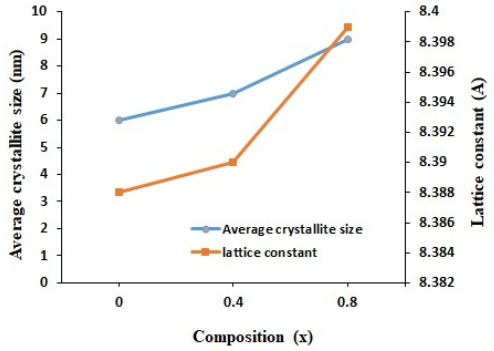

Fig. 2. The variations of the average crystallite size and lattice constant as a function of x values for un-calcined samples

As Table 1, the lattice constant slightly increased with the addition of x contents. The variation among the substitution cations and host ions radii and the distributed cations in the A and B sites can be affected by the lattice constant [20]. Furthermore, the variations of lattice constant lead to the variation distances among magnetic ions, the variations in the interactions, and the magneto behaviors of samples [21]. The enhancement of lattice constant can be discussed by the ionic radii. The radii of Mn^{2+} (0.91 Å), Co^{2+} (0.82 Å), Ni^{2+} (0.78 Å), and Cu^{2+} (0.70 Å) are larger than that of Fe^{3+} (0.63 Å). With the replacement of Fe^{3+} by Mn^{2+}, Co^{2+}, Ni^{2+}, and Cu^{2+}ions the unit cell increases, which increases the lattice constant [22-24]. Thus, among un-calcined ferrites, the mean crystallite size and lattice constant of the x=0.8 ferrite are bigger than others.
Fig. 3 illustrates the FESEM micrographs for un-calcined samples.

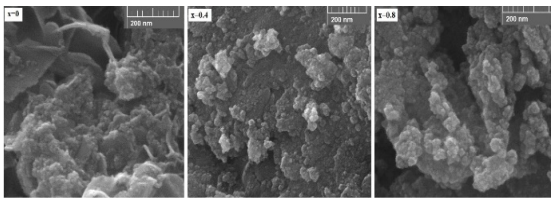

Fig. 3. FESEM images of un-calcined $Zn_{1-x}Fe_{1.2}[(Mn_xNi_{1-x})_{0.8}(Co_xCu_{1-x})_{0.2}]_{x+0.8}O_4$ with x equals to: 0, 0.4 and 0.8

The FESEM images show that the crystallites are narrowly distributed, the particles are agglomerated and are nearly spherical in shape. The interaction between magnetic particles causes agglomeration [24, 25].
The effect of Mn, Co, Ni, and Cu contents on the average particle size is shown in Fig. 4. As can be seen, with the enhancement of Mn, Co, Ni, and Cu contents, the average particle size increased in the range of 11-14 nm, as listed in Table 1. The enhancement of average particle size with increasing Mn, Co, Ni, and Cu contents is attributed to the increase in lattice constant.

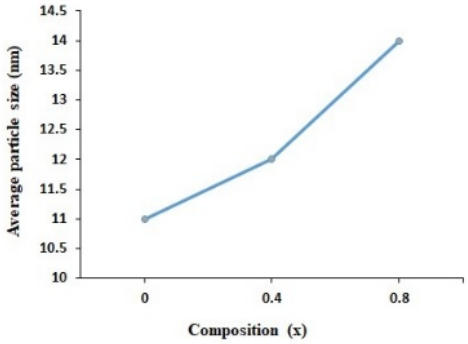

Fig. 4. The variations of the average particle sizes concerning x values for un-calcined samples

The size of particles measured by FESEM is bigger than the crystallite size calculates by Scherer's equation. Actually, each particle is formed by two aggregation crystallites [24, 25].

3.2. Magnetic properties

The changes of the magnetization based on coercivity field curve for un-calcined samples at room temperature and magnetic field of 8 kOe are exhibited in Fig. 5. It is showed that M_S is not attained for the un-calcined ferrites. To reach Ms, the samples are calcined at 900°C. As seen From Fig. 6 the magnetization of calcined samples is saturated.

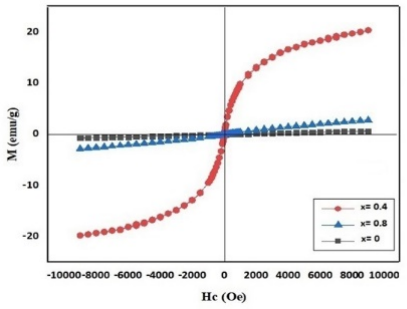

Fig. 5. M-H curve for un-calcined samples

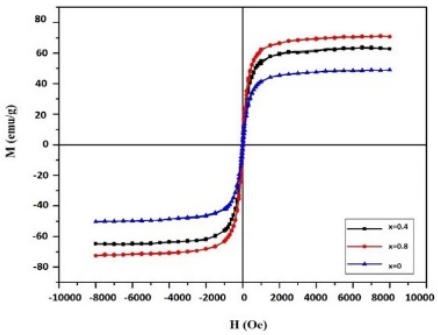

Fig. 6. M-H curve for calcined samples

The saturation magnetization (M_s) and remanent magnetization (M_r) for calcined ferrites at 900°C, maximum magnetization for an un-calcined sample (M_{max}), and coercivity field (H_c) for un-calcined and calcined samples are given in Table 2.

TABLE. 2. Magnetic parameters for un-calcined and calcined samples

Composition (x)	Calcination	0.0	0.4	0.8
Maximum magnetization (M_{max}), emu/g	Un-calcined	0.66	20.42	2.8
Coercivity field (H_c), Oe	Un-calcined	40.1	60.4	20.2
Saturation magnetization (M_s), emu/g	Calcined at 900◦C	48.99	62.73	70.74
Coercivity field (H_c), Oe	Calcined at 900◦C	19.20	17.31	16.4
Remanent magnetization (M_r), emu/g	Calcined at 900◦C	16.25	19.42	21.73
Squareness ratio (M_r/M_s)	Calcined at 900◦C	0.33	0.31	0.30

M_s is affected by the cations stoichiometry, particle spins canting, influence of the surface, crystallite size, interactions among cations, and disordered layer [5].

The changes of magnetization based on x composition for un-calcined and calcined samples are indicated in Fig. 7. The magnetization of calcined samples (M_s) is found more than un-calcined ones (M_{max}). Besides, the saturation magnetization rose as the x values increased. Thus, saturation magnetization for the calcined sample with x=0.8 is 70.74 (emu/g), more than that reported for others.

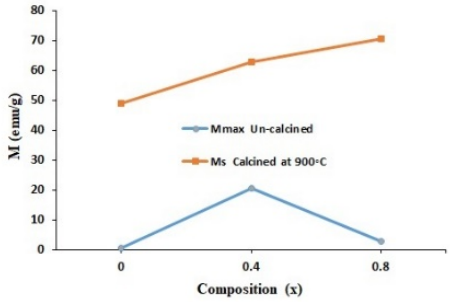

Fig. 7. The changes of magnetization based on x composition for un-calcined and calcined samples

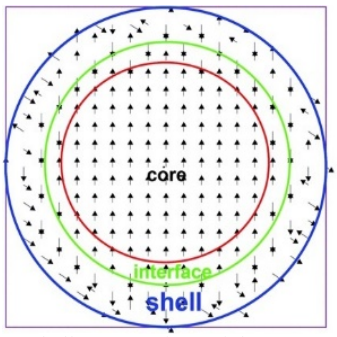

Fig. 8. Core-shell structure in particle

The increase of saturation magnetization may be due to the large size of grains and the wide degree of particles coarsening at higher temperatures in the calcined samples rather than un-calcined samples [22]. Also, it can be ascribed to the structure of the dead layer at the surface of the o particle. The structure of the layer is dependent on the superficial spins canting, high anisotropy layer, or loss of the long-range order in the surface layer [26].

Based on core-shell model as shown in Fig. 8, every particle composed of a core with the spin ordering and a superficial layer with a constant thickness and without net magnetization, which is named the dead layer [27].

The chaotic spins of the surface layer are affected by the super-exchange bonds and dissimilar the symmetry of atoms near the superficial layer [27]. Thus, the increment of the surface-to-volume ratio in the particles lead to an enhancement in the dead layer and a reduction in M_s [28].

The increment of magnetization may be described by a theory belong to Neel [29]. As stated by theory, there be three type of interchange between the unpaired electrons in the A and B sites. The interchange amongst magnetic ions detected at the A-site, the interchange amongst ions detected at the B-site, and the interchange of ions at the A-site with those at the B-site. The A-B interchanges are the powerful and in which the queuing of all the magnetic spins at the A-site in one route and those at the B-site in the contrary route [29]. The super-exchange interchange between cations is related to the various condensations and magneto moments of Ni^{2+}, Mn^{2+}, Co^{2+}, and Cu^{2+} and the spin-canting of ions at A and B [22]. The net magnetic moment for $Zn_{1-x}Fe_{1.2}[(Mn_xNi_{1-x})_{0.8}(Co_xCu_{1-x})_{0.2}]_{x+0.8}O_4$ depends on the distribution of Fe^{3+} and Mn^{2+}, Co^{2+}, Ni^{2+} and Cu^{2+} ions between A and B sites. Actually, Ni^{2+} (2.3μB), Cu^{2+} (1μB), and Co^{2+} (2μB) ions tend to get B sites, while Zn^{2+} ions choose A sites. Fe^{3+} (5μB) and Mn^{2+} (5μB) ions also choose both sites [22, 25]. The increment in M_s with enhancement of x may be ascribed to the B site occupancy by Ni^{2+} (2.3μB), Cu^{2+} (1μB), and Co^{2+} (2μB), which is effected by the immigration of some Fe^{3+} from B sites to A sites and the reduction in the magnetization of B sites. Moreover, the enhancement of Mn^{2+} (5μB) ions in A sites causes the immigration of some Fe^{3+} from A to B sites and the reduction in the magnetization of A-site. Thus, the net magnetization grows with increment x content.

Besides, the increment in the lattice constant of ferrites results in the development of unit cell volume, which increases the inter-atomic distance between ions and have an effect on the magnetic behaviors. The structural and magnetic features of $Zn_{1-x}Fe_{1.2}[(Mn_xNi_{1-x})_{0.8}(Co_xCu_{1-x})_{0.2}]_{x+0.8}O_4$ are depend upon Ni^{2+}, Mn^{2+}, Co^{2+}, and Cu^{2+} cation doping percentage.

The remanent magnetization (M_r) values of the calcined samples increase with an enhuncement in the x values and mean size of particle, which is attributed to the effects of surface in these particles. The modality of particles may be reached by measuring the squareness ratio by the following relation [30].

$$Squareness\ ratio = \frac{M_r}{M_s} \quad (1)$$

The calculated values for the squareness ratio are reported in Table 2. A decrease in the squareness ratio from 0.33 to 0.30 is observed with increment x values. This behavior is attributed to magnetocrystalline anisotropy [30].

The dependence of the coercivity (H_c) as a function of x contents for un-calcined and calcined samples is shown in Fig. 9. The results indicate that H_c is dependent on the anisotropy, particle size, and grain boundaries [10, 23]. It straightly changes with the porosity and reversely with grain sizes. The displacement of Fe^{3+} with Ni^{2+}, Co^{2+}, and Cu^{2+} ions at B sites cause the changes of useful anisotropy constant and H_c [31]. The diminution of H_c in un-calcined and calcined ferrites may be due to the formaition of multi-domain [32]. In this structure, H_c reduce with increasing size of particles [33].

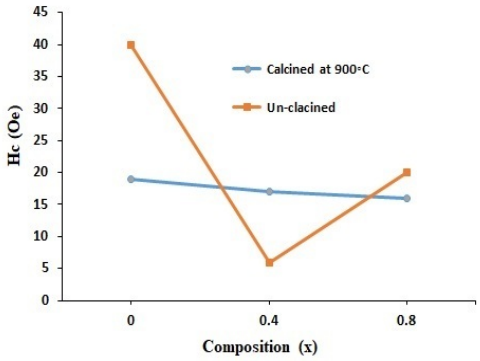

Fig. 9. The variations of coercivity a function of x for calcined and un-calcined samples

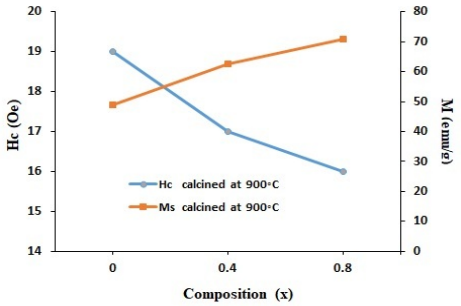

Fig. 10. The variations of coercivity and magnetization for calcined $Zn_{1-x}Fe_{1.2}[(Mn_xNi_{1-x})_{0.8}(Co_xCu_{1-x})_{0.2}]_{x+0.8}O_4$ as a function of x

In Fig. 10, amongst calcined ferrites, the x=0.8 calcined has lower coercivity than other calcined ones. Thus, this sample is appropriate for high-frequency applications, because of the maximum saturation magnetization and minimum coercivity.

The magnetic parameters obtained for samples were compared with the different research for samples prepared from various processes under previous conditions [34-36], as reported in Table 3. The results indicate that M_s and H_c depend on the preparation method, processing conditions, and exchange interactions between cations [22, 33-36].

The conclusion obtained by Khedri and Gholizadeh [34] display the connection of magnetization on the A–B exchange interactions. The magnetic parameters show a super-paramagnetic behavior in the samples. The samples with a smaller size of crystal than others have a higher portion ratio of the superparamagnetic to the ferromagnetic.

Dhiman et al [35] explain the decrease in the value of M_s on based on the various magnetic moments of A and B sublattices.

The results reported by Hossain et al [36] indicate the various values of M_s based on the distribution of Zn-ions in A and Fe between the A and B sites.

TABLE. 3**.** Contents of D, M_s, and H_c reported for different ferrites [34], [35], [36].

Sample	Method & calcination	D (nm)	M_S (emu/g)	H_c (Oe)
Cu0.5Zn0.5Fe2O4	Citrate 500 °C 2 h	14.61	2.393	10.46
Mn0.3Cu0.2Zn0.5Fe2O4		9.99	1.328	1.08
Fe0.3Cu0.2Zn0.5Fe2O4		11.30	1.726	17.90
Co0.3Cu0.2Zn0.5Fe2O4		13.24	2.176	67.53
Ni0.3Cu0.2Zn0.5Fe2O4		19.21	2.831	35.21
CoMn0.4Co0.2Fe1.4O4	sol–gel auto combustion 400°C 2 h	53	31.59	330
CoMn0.4Ni0.2Fe1.4O4		52	26.25	157
CoMn0.4Cu0.2Fe1.4O4		52	23.53	500
CoMn0.4Zn0.2Fe1.4O4		52	23.93	230
Ni0.2Cu0.3Zn0.5Fe2O4	sol–gel auto combustion 700°C 4 h	22.95	49.83	32.75
Ni0.3Cu0.3Zn0.4Fe2O4		29.96	66.07	21.72
Ni0.4Cu0.3Zn0.3Fe2O4		29.92	49.31	16.87
Ni0.5Cu0.3Zn0.2Fe2O4		29.17	36.19	43.97

4. CONCLUSIONS

The end of the paper should conclude with a brief conclusion of the manuscript's contents and contribution and also mention future research recommendations.

The effect of Mn, Cu, Ni, and Co substitution on the behaviors of $Zn_{1-x}Fe_{1.2}[(Mn_xNi_{1-x})_{0.8}(Co_xCu_{1-x})_{0.2}]_{x+0.8}O_4$ (x= 0, 0.4 and 0.8) samples have

investigated. XRD study showed a single-phase fcc formation in ferrites and the increase in mean size of crystal and lattice constant with the increment of x values. From FESEM images, the average particle size was determined 11-14 nm. The hysteresis studies showed that the magnetization of the calcined samples is more than the un-calcined ones. Also, by doping Mn, Cu, Ni, and Co ions on zinc ferrite, the magnetization increased. Analysis of the magneto behaviors of ferrites related to the core-shell model displayed that the decline of size of particles lead to the increment of the surface-to-volume ratio, which cause the reduction in M_s. Amongst ferrites, the x=0.8 calcined, due to its biggest size of particle, evidenced the higher magnetization than others. The remanent magnetization of the calcined ferrites grow with an enhuncement in mean size of particle. This is ascribe to the influence of the surface in these particles. The quality of particles was achieved with a squareness ratio of about 0.30-33. Besides, the increase of magnetization in calcined samples were explained by Neel's theory. The replacement of Fe^{3+} and Zn^{2+} cations by Ni^{2+}, Mn^{2+}, Co^{2+}, and Cu^{2+} ions increased in the net magnetic moment, the magnetization in B site was increased. Fe^{3+} replacement by Ni^{2+}, Mn^{2+}, Co^{2+}, and Cu^{2+} ions resulted in variations of the effective anisotropy constant and coercivity. The decrease in coercivity with enhuncement of x composition evidented the multi-domain formation of ferrites. Amongst ferrites, the un-calcined x=0.4 ferrite had the lowest coercivity, while the x=0.8 calcined had a lower coercivity than other calcined samples. Thus, the co-precipitation method is suitable for obtaining fine nanoparticles, and Ni, Mn, Co, and Cu replacement zinc ferrite changes them to materials with soft magnetic structure. Besides, the calcined samples are used for applications with high-frequency.

5. ACKNOWLEDGMENT

This work was augmented at Malek Ashtar University of Technology and was supported by Niroo Research Institute. We are thankful to the institute for their support.

REFERENCES

[1] A. Ghasemin and M .Mousavinia. 2014. "Structural and magnetic evaluation of substituted $NiZnFe_2O_4$ particles synthesized by conventional sol–gel method," *Ceram. Int.,* Vol. 40(2), P: 2825–2834.

[2] H. Hao, P. Donghua and L. Duxin. 2019. "Study on Fe–Si–Cr Soft magnetic composite coated with silicon dioxide," *Mater. Res. Express.,* Vol. 6, P: 26104.

[3] P. Mathur, A. Thakur, J.H. Lee and M. Singh. 2010. "Sustained electromagnetic properties of Ni–Zn–Co nanoferrites for the high-frequency applications," *Mater. Lett.,* Vol. 64(24), P: 2738–2741.

[4] Y.Y. Meng, Z.W. Liu, H.C. Dai, H.Y. Yu, D.C. Zeng, S .Shukla and R.V. Ramanujan. 2012. "Structure and Magnetic Properties of $Mn(Zn)Fe_2O_4$ Ferrite Nano-Powders Synthesized by Co-Precipitation and Refluxing Method," *Powder Technol.,* Vol. 229, P: 270–275.

[5] A. Gholizadeh and E. Jafari. 2017. "Effects of sintering atmosphere and temperature on structural and magnetic properties of Ni-Cu-Zn ferrite nano-particles: Magnetic enhancement by a reducing atmosphere," *Magn. Magn. Mater.,* Vol. 422, P: 328.

[6] Z. Beji, T. Ben Chaabane, L. S. Smiri, S. Ammar, F. Fiévet, N. Jouini and J. M. Grenèche. 2006. "Synthesis of nickel–zinc ferrite nanoparticles in polyol: morphological, structural and magnetic studies," *App. Mate. Sci.,* Vol.203, P: 504-512.

[7] N. Kaur and M Kaur. 2014. "Comparative studies on impact of synthesis methods on structural and magnetic properties of magnesium ferrite nanoparticles," *Proc. Appli. Ceram.,* Vol. 8 (3), P: 137-143.

[8] K. Rana, P. Thakur, P. Sharma, M. Tomar, V. Gupta and A. Thakur. 2015. "Improved structural and magnetic properties of cobalt nanoferrites: influence of sintering temperature," Ceram. Int., Vol. 41, P: 4492-97.

[9] Y. Qu, H. Yang, N. Yang, Y. Fan, H. Zhu and G. Zou. 2006. "The effect of reaction temperature on the particle size, structure and magnetic properties of coprecipitated $CoFe_2O_4$ nanoparticles," *Matter. Lett.,* Vol. 60, P: 3548.

[10] F. Ghanbari, A. Arab, M. Shishe Bor and M.R Mardaneh. 2017. "Magnetic Properties of La/Ni-Substituted Strontium Hexaferrite Nanoparticles Prepared by Coprecipitation at Optimal Conditions," *Electron. Mater.,* Vol. 46(4), P: 2112–2118.

[11] O.M. Hemeda, A. Tawfik, M. Mostafa, M. Zaki and M.I. Abd El Ati. 2019. "Structural and magnetic properties of nano ferrite for magnetoelectric applications," *Phys: Conf. Series.,* Vol. 1235, P: 012026.

[12] A. Pathania, P. Thakur, A.V. Trukhanov, S.V. Trukhanov, L.V. Panina, U. Lüders and A. Thakur. 2019. "Development of tungsten doped Ni-Zn nano-ferrites with fast response and recovery time for hydrogen gas sensing application," *Results. Phys.,* Vol. 15, P: 102531.

[13] A. Pathania, S. Bhardwaj, S. Singh Thakur, J.L. Mattei, P. Queffelec, L.V. Panina, P. Thakur and A. Thakur. 2018. "Investigation of structural, optical, magnetic and electrical properties of tungsten doped NiZn nano-ferrites," *Phys B: Cond. Matter.,* Vol.531, P: 45-50.

[14] J. Hu, X. Liu, X. Kan, S. Feng, C. Liu, W. Wang, M. Khalid, M. Shazed, S. Zhou and Q. Wu. 2019. "Characterization of Texture and Magnetic Properties of $Ni_{0.5}Zn_{0.5}TiFe_2O_4$ Spinel Ferrites," *Magn. Magn. Mater.*, Vol. 489, P: 165411.

[15] G. S. Shahane, A. Kumar, M. Arora, R.P. Pant and K. Lal. 2010. "Synthesis and characterization of Ni–Zn ferrite nanoparticles," *Magn. Magn. Mate.,* Vol. 322, P: 1015-1019.

[16] S. Rehman, K. Nadeem, M. Anis-ur-Rehman, M. Mumtaz, S. Naeemal and I. Letofsky-Papstc. 2013. "Structural and Magnetic Properties of ZnMg-Ferrite Nanoparticles Prepared Using the Co-Precipitation Method," *Ceram. Int.*, Vol. 39, P: 5235-5239.

[17] M. C. Dimri, S. Kashyap, A. Verma and C. Dube. 2006. "Structural, Dielectric and Magnetic Properties of NiCuZn Ferrite Grown by Citrate Precursor Method," *Mate. Scie. Engi.,* Vol. 133(1-3), P: 42-48.

[18] A. Lassoued, M.B. Hassine, F. Karolak and B. DKhil, 2017. "Synthesis and magnetic characterization of Spinel ferrites MFe_2O_4 (M = Ni, Co, Zn and Cu) via chemical co-precipitation method," Vol. 28, P: 28.

[19] Th. Tnacharon, A. Ruangphanit and W. Pecharapa. 2013. "zinc-doped metal ferrites (metal = Ni; Mn; Cu) prepared by sol-gel combustion method," *Ceram. Int.*, Vol. 39, P: S239-S243.

[20] S.E. Jacobo and P.G. Bercoff. 2016. "Structural and electromagnetic properties of yttrium-substituted Ni–Zn ferrites," *Ceram. Int.,* Vol. 42, P: 7664- 7668.

[21] K. Verma, A. Kumar and D. Varshney. 2013. "Effect of Zn and Mg doping on structural, dielectric and magnetic properties of tetragonal $CuFe_2O_4$," *Curr. Appl. Phys.,* Vol. 13(3), P: 467- 473.

[22] S. Shafiee, A. Arab and N. Riahi-Nouri. 2021, "Enhanced magnetic permeability in $Ni_{12x}(Zn_{0.6}Mg_{0.2}Cu_{0.2})_xFe_2O_4$ synthesized by auto combustion method," *Bull. Mater. Sci.,* Vol. 2021, P: 44-141.

[23] D.H. Yoon, M. Raju and K. Raju. 2016. "Controlling the Magnetic Properties of Nickel Ferrites by Doping with Different Divalent Transition Metal (Co, Cu, and Zn) Cations," *Supercond. Nov. Magn.,* Vol. 29, P: 439-445.

[24] R.S. Alam, M. Moradi, M. Rostami, H. Nikmanesh, R. Moayedi and Y. Bai. 2015. "Structural, magnetic and microwave absorption properties of doped Ba-hexaferrite nanoparticles synthesized by co-precipitation method," *Magn. Magn. Mater.,* P: 381.

[25] J. Pei and Z. Wang, 2018. "Effect of Bi-Co co-doping on the microstructure and magnetic properties of NiMgCuZn ferrites," *Magn. Magn. Mater.,* Vol. 465, P: 598.

[26] T. Maehara, K. Konishi, T. Kamimori, H. Aono, H. Hirazawa, T. Naohara, S. Nomura, H. Kikkawa, Y. Watanabe and K. Kawachi. 2005. "Selection of ferrite powder for thermal coagulation therapy with alternating magnetic field," *Mater. Sci.,* Vol. 40, P: 135-138.

[27] M. Sertkol, Y. Köseoğlu, A. Baykal, H. Kavas and A.C. Başaran. 2009. "Enhanced magnetic Properties of $MgFe_2O_4$ nanoparticles," *Magn. Magn. Mater.,* Vol. 321, P: 157.

[28] I. Maghsoudi, H. Shokrollahi, M.J. Hadianfard, J. Amighian. 2013. "Synthesis and characterization of $NiAl_xFe_{2-x}O_4$ magnetic spinel ferrites produced by conventional method," *Powd. Tech.,* Vol. 235, P: 110.

[29] DRS. Gangaswamy, GSV. RK. Choudary, M. Chaitanya Varma, S. Bharadwaj, KH. Rao. 2018. "Enhanced Magnetic Permeability in $Ni_{0.55-y}Co_yZn_{0.35}Mg_{0.10}Fe_2O_4$ Synthesized by Sol-Gel Method," *Supercond. Nov. Magn.,* Vol. 31, P: 3753-3760.

[30] R. Topkaya, A. Baykal and A. Demir. 2013. "Yafet–Kittel-type magnetic order in Zn-substituted cobalt ferrite nanoparticles with uniaxial anisotropy," *Nanoparticle Res.,* Vol. 15, P: 1359.

[31] N. Rezlescu, C. Doroftei, E. Rezlescu and P.D. Popa. 2008. "The influence of heat-treatment on microstructure and magnetic properties of rare-earth substituted $SrFe_{12}O_{19}$," *Alloys. Compd.,* Vol. 451, P: 492-496.

[32] M. George, A. M. John, S. S. Nair, P. A. Joy and M. R. Anantharaman, "Finite Size Effects on the Structural and Magnetic Properties of Sol-Gel Synthesized NiFe2O4 Powders," *Magn. Magn. Mater.,* Vol. 302, P: 190-195.

[33] H. Arabi and F. Ganjali. 2013. "Structural and magnetic properties of cobalt and manganese doped Ni-ferrite nanoparticles," *Supercond. Nov. Magn.,* Vol. 26, P: 1031–1035.

[34] H. Khedri and A. Gholizadeh, 2019. "Experimental comparison of structural, magnetic and elastic properties of $M_{0.3}Cu_{0.2}Zn_{0.5}Fe_2O_4$ (M = Cu, Mn, Fe, Co, Ni, Mg) nanoparticles," *Appl. Phys. A.,* Vol. 125, P: 709.

[35] M. Dhiman, S. Bhukal, B. Chudasama and S. Singhal, 2017. "Impact of metal ions (Cr^{3+}, Co^{2+}, Ni^{2+}, Cu^{2+} and Zn^{2+}) substitution on the structural, magnetic and catalytic properties of substituted Co–Mn ferrites synthesized by sol–gel route," *Sol-Gel. Sci. Tech.,* Vol. 81, P: 831–843.

[36] M. S. Hossain, Y. Akter, M. Shahjahan, M. Shahriar Bashar, M. H. Ara Begum, M. Moazzem Hossain, S. Islam, N. Khatun and M. Al-Mamun, 2019. " Influence of Ni substitution on structural, morphological, dielectric, magnetic and optical properties of Cu–Zn ferrite by double sintering sol–gel technique," *Adva. Diel.,* Vol. 9 (2).